Evolutionary characteristic length method for smeared cracking finite element models

Khalid M. Mosalam[a,*], Glaucio H. Paulino[b,1]

[a] *School of Civil and Environmental Engineering, Cornell University, Ithaca NY 14853-3501, USA*
[b] *Department of Civil and Environmental Engineering, University of California, Davis, CA 95616-5294, USA*

Dedicated to Professor Peter Gergely (*in memoriam*)

Abstract

The fixed smeared crack concept with strain decomposition is reformulated utilizing a self-adaptive strategy at the constitutive level. This formulation focuses on continuous adaptation of the *crack band width* based on the incremental finite element solution and the idea of nonlocal continuum. The required nonlocal forms are obtained by means of the superconvergent patch recovery procedure. Comparison with experimental results indicates the superiority of the present formulation over the standard smeared cracking. © 1997 Elsevier Science B.V.

1. Introduction

One of the fundamental components in nonlinear problems undergoing localized damage is the existence of an internal length parameter. This characteristic length determines *the width of the localization zone*. In smeared cracking terminology, this length parameter is the *crack band width* (w_c). When this parameter is related to the adopted finite element size, the spurious mesh dependency on the structural load–deformation response can be eliminated. The relation between w_c and the finite element size can be determined by trial-and-error fitting of some reliable results (e.g. experimental results or selected discrete crack results [1]). Some ad hoc rules depending on the chosen element type, element size, element shape, integration scheme and even on the particular problem considered, can be established to determine w_c. In the existing literature, Bažant [2] and Oliver [3] have attempted to rationalize the arbitrariness of the choice of the crack band width. In [2], Bažant has used stability analysis to determine w_c. As he states, this stability analysis seems useful in principle, but not in practice, as it is not known how to perform this analysis. In [3], Oliver has analyzed a singular band in a two-dimensional (2D) domain, in which a crack is modeled as

---

* Corresponding author.
[1] Formerly, Research Assistant, School of Civil and Environmental Engineering, Cornell University.

a limiting case of two singular lines with continuous displacements but discontinuous gradients across them. This allowed him to relate the crack band width to the crack orientation and the characteristics of the finite element interpolation functions. Although this approach is interesting, it renders the estimated value of the crack band width *constant* throughout the entire loading history.

In many applications, upon increasing the damage level (determined here by the crack strain), cracking tends to *localize in a band of decreasing width.* By simply relating w_c to the finite element size (in 2D problems, the finite element area, A_e), one *cannot* capture such decrease of this band upon increase of the damage. A remedy to such shortcoming is to *adapt* the finite element mesh to the present level of damage (cracking). Accordingly, the element size is determined in a manner consistent to the nature of the localization process. Upon such automated adjustment of the finite element size, a simple rule for the crack band width, e.g. $w_c \propto \sqrt{A_e}$, may be sufficient for accurately capturing localization. This adaptation requires continuous modification of the topology of the finite element mesh and needs a robust *transfer operator* [4]. Unfortunately, such tasks in a highly nonlinear problem are difficult to execute. In this paper, a practical adaptation of the crack band width, without any change in the topology of the finite element mesh, is developed. In this process, the *crack band width* is treated as a material parameter in the constitutive model, which greatly simplifies the technique.

2. Smeared cracking

Smeared cracking is a continuum approach for fracture mechanics in which local discontinuities are distributed (i.e. smeared) over a certain tributary area within the finite element. Accordingly, crack strain can be defined as a function of the relative displacement (displacement jump or displacement discontinuity) of the crack surfaces and some length parameter over which this displacement jump is distributed. The introduction of such *characteristic length* allows modeling of the cracked material in terms of stress–strain relations.

Since the advent of the smeared crack concept by Rashid [5], it has been refined by several researchers [6]. Significant improvements of the smeared crack concept have been provided by *the fictitious crack model* developed by Hillerborg et al. [7] and *the crack band theory* developed by Bažant and Oh [8]. In the fictitious crack model, the tensile strength (f_t) and the fracture energy ($\mathscr{G}_f$) are the model parameters. The fracture energy is the amount of energy required to create one unit area of crack surface. The two parameters (f_t and $\mathscr{G}_f$) are also included in the crack band theory, in addition to a third parameter, termed the crack band width (w_c).

The modern approach for smeared cracking models is based on the idea of *strain decomposition* (e.g. [1]). In this idea, an increment of the total strain vector $\Delta\varepsilon$ is decomposed into an increment of the crack strain vector $\Delta\varepsilon_{cr}$ and an increment of the solid material (i.e. material between cracks) strain vector $\Delta\varepsilon_{ma}$, i.e.

$$\Delta\varepsilon = \Delta\varepsilon_{cr} + \Delta\varepsilon_{ma}. \tag{1}$$

Note that in Eq. (1) and the sequel, bold face letters indicate matrix type quantities. The above concepts are illustrated by Fig. 1. Consider a Gauss point in one element (Fig. 1(a)) of the mesh. The principal stresses (σ_1, σ_2) can be obtained by means of the Mohr circle (Fig. 1 (b)). Next, the *cracking*
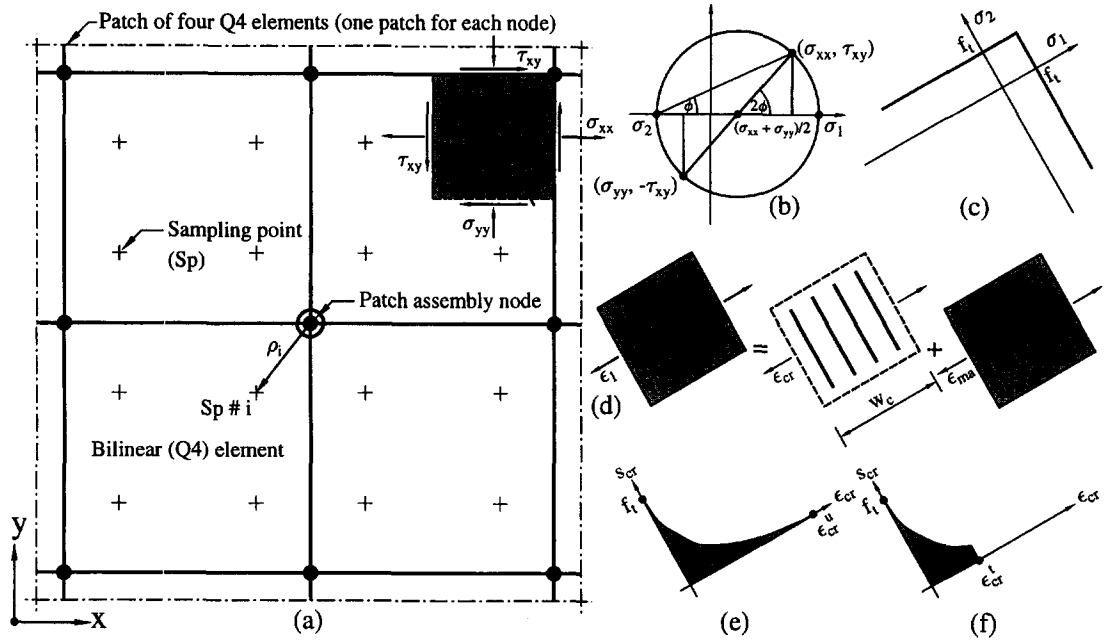
Fig. 1 Smeared cracking and superconvergent patch recovery (SPR) technique: (a) example of a patch; (b) Mohr circle; (c) tension cut-off in 2D principal stress space; (d) strain decomposition; (e) total fracture energy density (full cracking); (f) apparent fracture energy density (partial cracking).

criterion, as determined by the Rankine failure surface of Fig. 1(c), is checked. If cracking occurs, then the strains are decomposed according to Eq. (1), as shown in Fig. 1(d).

A family of crack normal stress versus crack normal strain ($s_{cr} - \varepsilon_{cr}$) relations is considered in this study. This family is based on curve-fitting of a large number of experiments, as reported by Reinhardt [9], to determine the crack normal stress versus crack opening ($s_{cr} - \delta_{cr}$) relations of concrete. This family of relations is governed by the exponent k in the following equation:

$$\frac{s_{cr}}{f_t} = 1 - \left(\frac{\delta_{cr}}{\delta_{cr}^u}\right)^k,$$ (2)

where δ_{cr}^u is the stress-free crack opening (i.e. opening at total loss of load carrying capacity). This crack opening can be related to *the total fracture energy* ($\mathcal{G}_f$) by considering the following relation:

$$\mathcal{G}_f = \int_0^{\delta_{cr}^u} s_{cr}\, d\delta_{cr}.$$ (3)

This definition implies that $\mathcal{G}_f$ is the area under the stress versus crack opening graph. From Eqs. (2) and (3), one easily obtains

$$\delta_{cr}^u = \frac{(k + 1)\mathcal{G}_f}{k f_t}.$$ (4)

Assuming uniform distribution of the crack opening over w_c, one gets the following simple and important relationship (see Fig. 1(d))

$$\varepsilon_{cr} = \frac{\delta_{cr}}{w_c}. \tag{5}$$

Substitution of Eqs. (4) and (5) into Eq. (2) leads to

$$s_{cr} = f_t \left(1 - \left(\frac{k f_t w_c \varepsilon_{cr}}{(k+1) \mathscr{G}_f} \right)^k \right), \tag{6}$$

which gives the softening (descending) branch of a smeared crack in terms of the basic three parameters of the previously mentioned crack band theory [8], namely f_t, $\mathscr{G}_f$ and w_c. From the assumption stated by Eq. (5) and for constant w_c, one obtains the (total) fracture energy density as

$$g_f = \int_0^{\varepsilon_{cr}^u} s_{cr} \, d\varepsilon_{cr} = \mathscr{G}_f / w_c, \tag{7}$$

where g_f is the total area under the stress versus crack strain graph (cf. with Eq. (3)), as illustrated by Fig. 1(e). The *apparent fracture energy density* (g^t), shown in Fig. 1(f), is the fracture energy density determined at a particular load level (t), i.e.

$$g^t = \int_0^{\varepsilon_{cr}^t} s_{cr} \, d\varepsilon_{cr}, \tag{8}$$

which is the *partial* area under the stress versus crack strain graph (see Fig. 1(f)).

3. Local and nonlocal apparent fracture energy

The nonlocal continuum is an approach for which at least some variables are defined by *spatial averaging* [10]. Here, the *apparent fracture energy density* g^t (see Fig. 1(f)) is first established on the local level, i.e. in terms of the pointwise strains and crack band widths. Then, this form is generalized to give a nonlocal expression for g^t, which is called $\bar{g}^t$, in terms of nonlocal quantities which are the spatial averaging (smoothing) of their equivalent local ones. The smoothing process, required to obtain the spatially averaged quantities, is described in the next section.

After simplification, Eqs. (6) and (8) lead to

$$g^n = f_t \left(\varepsilon_{cr}^n - \frac{1}{k+1} \left(\frac{k f_t}{(k+1) \mathscr{G}_f} \right)^k \sum_{i=1}^{n} [\Delta_i^k (\varepsilon_{cr}) (w_c|_i)^k] \right), \tag{9}$$

where n is the number of load increments up to the load level t, $w_c|_i$ is the constant crack band width during increment i, and the operator Δ_i^k is defined as

$$\Delta_i^k(\bullet) = (\bullet^i)^{k+1} - (\bullet^{i-1})^{k+1}. \tag{10}$$

Eq. (9) gives the local form of the *apparent fracture energy density*. The nonlocal form of such quantity ($\bar{g}^t$) is similar to Eq. (9) but expressed as a function of the nonlocal crack strain ($\bar{\varepsilon}_{cr}$) and

a nonlocal form of the crack band width ($\bar{w}_c$). This function is given by

$$\bar{g}^n = f_t\left(\bar{\varepsilon}_{cr}^n - \frac{1}{k+1}\left(\frac{kf_t}{(k+1)\mathcal{G}_f}\right)^k \sum_{i=1}^{n}[\Delta_i^k(\bar{\varepsilon}_{cr})(\bar{w}_c|_i)^k]\right) \tag{11}$$

Subtracting Eq. (9) from Eq. (11), one obtains

$$\mathcal{E}_g = f_t\left(\mathcal{E}_{\varepsilon_{cr}} - \frac{1}{k+1}\left(\frac{kf_t}{(k+1)\mathcal{G}_f}\right)^k \sum_{i=1}^{n}[\Delta_i^k(\bar{\varepsilon}_{cr})(\bar{w}_c|_i)^k - \Delta_i^k(\varepsilon_{cr})(w_c|_i)^k]\right), \tag{12}$$

where

$$\mathcal{E}_g = \bar{g}^n - g^n \quad \text{and} \quad \mathcal{E}_{\varepsilon_{cr}} = \bar{\varepsilon}_{cr}^n - \varepsilon_{cr}^n \tag{13}$$

are measures of the *local errors* (see, for example, Refs [4, 11]) for the apparent fracture energy density and the crack strain, respectively. From Eq. (12), an expression for the nonlocal crack band width after n load increments, or for the new load level $(t + 1)$, is readily obtained as

$$w_c^{t+1} = \bar{w}_c|_n$$

$$= \left(\frac{(k+1)\left(\frac{(k+1)\mathcal{G}_f}{kf_t}\right)^k\left(\mathcal{E}_{\varepsilon_{cr}} - \frac{\mathcal{E}_g}{f_t}\right) - \sum_{i=1}^{n-1}[\Delta_i^k(\bar{\varepsilon}_{cr})(\bar{w}_c|_i)^k] + \sum_{i=1}^{n}[\Delta_i^k(\varepsilon_{cr})(w_c|_i)^k]}{\Delta_n^k(\bar{\varepsilon}_{cr})}\right)^{1/k}. \tag{14}$$

This is the evolution equation for the crack band width.

Assuming $\Delta_i^k(\varepsilon_{cr}) \approx \Delta_{i-1}^k(\bar{\varepsilon}_{cr})$ and setting $w_c|_i = \bar{w}_c|_{i-1}$, a simpler form of Eq. (14) is obtained as

$$w_c^{t+1} = \bar{w}_c|_n = \left(\frac{(k+1)\left(\frac{(k+1)\mathcal{G}_f}{kf_t}\right)^k\left(\mathcal{E}_{\varepsilon_{cr}} - \frac{\mathcal{E}_g}{f_t}\right) + \Delta_1^k(\varepsilon_{cr})(w_c|_1)^k}{\Delta_n^k(\bar{\varepsilon}_{cr})}\right)^{1/k}. \tag{15}$$

Note that $\Delta_1^k(\varepsilon_{cr}) = (\varepsilon_{cr}^1)^{k+1}$, which comes from the fact that the counter i in Eq. (10) starts at the onset of cracking.

4. Nonlocal forms and superconvergent patch recoveries

The nonlocal forms for the apparent fracture energy density and the crack strain, denoted by $\bar{g}^t$ and $\bar{\varepsilon}_{cr}^t$, respectively, are obtained by means of a spatial averaging of their local forms. To obtain these nonlocal forms, the superconvergent patch recovery (SPR), originally proposed by Zienkiewicz and Zhu [11], is employed here.

The fields $\bar{g}^t$ and $\bar{\varepsilon}_{cr}^t$ can be approximated by the *polynomial expansions*

$$\bar{g}^t = \mathcal{P}a \quad \text{and} \quad \bar{\varepsilon}_{cr}^t = \mathcal{P}c, \tag{16}$$

where $\mathcal{P}$ contains the appropriate polynomial terms, and both a and c are sets of unknown parameters. For 2D problems and bilinear (4-noded isoparametric) finite elements (see Fig. 1(a)),

the following approximation is recommended [11]

$$\mathscr{P} = [1 \ x \ y \ x \ y], \quad \boldsymbol{a} = [a_0 \ a_1 \ a_2 \ a_3]^{\mathrm{T}}, \quad \boldsymbol{c} = [c_0 \ c_1 \ c_2 \ c_3]^{\mathrm{T}} \tag{17}$$

The unknown coefficients $\boldsymbol{a}$ and $\boldsymbol{c}$ can be obtained through a *weighted least-square fit* of the *polynomial expansions* (16) to the values of g^{t} and $\varepsilon_{\mathrm{cr}}^{\mathrm{t}}$ obtained from the finite element solution at the sampling points, i.e. $\hat{g}^{\mathrm{t}}$ and $\hat{\varepsilon}_{\mathrm{cr}}^{\mathrm{t}}$. The finite element solution (e.g. stresses, strains or a combination of them such as the fracture energy density) at these sampling points is generally the most accurate one (i.e. superconvergent upon enhancing the interpolation or the discretization). Instead of applying the least square fit to the whole domain of the problem (*global fit*), Zienkiewicz and Zhu [11] have suggested the use of small *patches* of elements to perform *local* least-squares fit. This procedure is adopted here. However, a weighting parameter (w_i) is added to emphasize the influence of the sampling points which are closer to the patch assembly node (see Fig. 1(a)). Thus,

$$w_i = 1/\rho_i^p, \tag{18}$$

where ρ_i is the Euclidean distance between the sampling point i and the patch assembly node, and p is an integer. In practical applications, p is generally in the range from 0 to 4. The case $p = 0$ corresponds to the original SPR (with uniform weighting).

Consider a *patch* of elements containing m sampling points as illustrated by Fig. 1(a), in which $m = 16$. For a generic sampling point i in this patch, let (x_i, y_i) be the Cartesian coordinates in the global axes. Thus, the weighted least-squares problem reduces to the minimization of the following functionals:

$$\mathscr{F} = \sum_{i=1}^{m} w_i^2 [\bar{g}^{\mathrm{t}}(x_i, y_i) - \hat{g}^{\mathrm{t}}(x_i, y_i)]^2 \quad \text{and} \quad \mathscr{H} = \sum_{i=1}^{m} w_i^2 [\bar{\varepsilon}_{\mathrm{cr}}^{\mathrm{t}}(x_i, y_i) - \hat{\varepsilon}_{\mathrm{cr}}^{\mathrm{t}}(x_i, y_i)]^2, \tag{19}$$

where the terms in square brackets are analogous to the ones given by Eq. (13). Substituting expressions (16) into (19), and solving the minimization problem by setting

$$\partial \mathscr{F}/\partial \boldsymbol{a} = 0 \quad \text{and} \quad \partial \mathscr{H}/\partial \boldsymbol{c} = 0, \tag{20}$$

one obtains the following sets of linear algebraic equations:

$$\boldsymbol{A}\boldsymbol{a} = \boldsymbol{b} \quad \text{and} \quad \boldsymbol{A}\boldsymbol{c} = \boldsymbol{d}, \tag{21}$$

where

$$\boldsymbol{A} = \sum_{i=1}^{m} w_i^2 \mathscr{P}^{\mathrm{T}}(x_i, y_i) \mathscr{P}(x_i, y_i) \tag{22}$$

$$\boldsymbol{b} = \sum_{i=1}^{m} w_i^2 \mathscr{P}^{\mathrm{T}}(x_i, y_i) \hat{g}^{\mathrm{t}}(x_i, y_i), \qquad \boldsymbol{d} = \sum_{i=1}^{m} w_i^2 \mathscr{P}^{\mathrm{T}}(x_i, y_i) \hat{\varepsilon}_{\mathrm{cr}}^{\mathrm{t}}(x_i, y_i) \tag{23}$$

Since m is a small number compared to the actual problem size, the sets of simultaneous equations given by (21) can be easily solved for the unknown vectors $\boldsymbol{a}$ and $\boldsymbol{c}$.

5. Numerical implementation

The method for adapting the crack band width in the smeared cracking model has been implemented in the DIANA[2] (DIsplacement ANAlyzer) system. The main steps for this specific implementation are summarized as follows:

1. Determine the mesh and initialize the material parameters.
2. Compute $\hat{\varepsilon}_{cr}^n$ at the load increment n.
3. Calculate $\hat{g}^n$ (Eq. (9)) using the history of both the crack strain (ε_{cr}^i) and the corresponding crack band width ($w_c|_i$).
4. Solve the weighted least-squares minimization problems in the SPR procedure to obtain the fields $\bar{\varepsilon}_{cr}^n$ and $\bar{g}^n$.
5. Update the crack band width at each sampling point using either Eq. (14) or Eq. (15).
6. Continue the incremental iterative solution scheme until the final load step.

6. Numerical application

The crack-line-wedge-loaded double-cantilever-beam (CLWL-DCB), tested by Kobayashi et al. [12] and analyzed by Rots [1], is selected to check the validity of the proposed adaptive characteristic length method. Other examples will be presented elsewhere. The dimensions, material parameters and boundary conditions are illustrated in Fig. 2(a). In this figure, E and v are, respectively, Young's modulus and Poisson's ratio for the material of the specimen. The shear retention factor $\beta \approx 0.0$ is chosen as such to cause the axes of principal stress to remain *practically fixed* after crack formation. The specimen is assumed to be in a state of plane stress. The ratio of the diagonal force (F_2) to the wedge force (F_1) is kept approximately constant at 0.6 until $F_2 = 3.78\,\text{KN}$. Then, F_2 is kept constant and only F_1 is altered [12]. The diagonal force is applied under load control and the wedge loading under displacement control. The adopted finite element mesh is shown in Fig. 2(b), and consists of four node quadrilaterals (Q4) with two by two Gaussian integration. The transition from a coarser mesh to a finer one at the upper-right corner of the plate is achieved by using slave nodes along the mesh transition line. The reported results for this example have been obtained using Eq. (15) and considering $p = 2$ in Eq. (18). The double-directional fixed smeared cracking model has been adopted here, and the nonlinear finite element system of equations for this example is solved using the *Newton–Raphson* method where the tangential stiffness matrix is set up before each iteration. The convergence criterion for the equilibrium iteration process is based on checking the norm of the out-of-balance force vector ($\leqslant 10^{-3}$).

Fig. 3(a) shows the graph for the wedge force (F_1) versus the crack mouth opening displacement (CMOD). Note that a better agreement with the experimental results is achieved when the evolutionary characteristic length method (adaptive w_c) is used than when w_c is kept constant throughout the analysis (standard smeared cracking). At highly damaged states, e.g. CMOD $\geqslant 0.25\,\text{mm}$ in Fig. 3(a), there is a departure from the adapted and experimental results.

---

[2] DIANA is a finite element code developed at TNO Building and Construction Research in The Netherlands.

thickness = 50.8 mm
$F_2 / F_1 \approx 0.6 \quad \forall F_2 \leq 3.78$ KN
dimensions in mm

$E = 30$ KN/mm^2
$\nu = 0.2$
$f_1 = 3.0$ N/mm^2
$G_f = 100$ J/m^2
$\beta = 0.001$
$k = 0.31$

g^t contours in this region
are shown in Fig. (4)

• Slave nodes

(a)   (b)
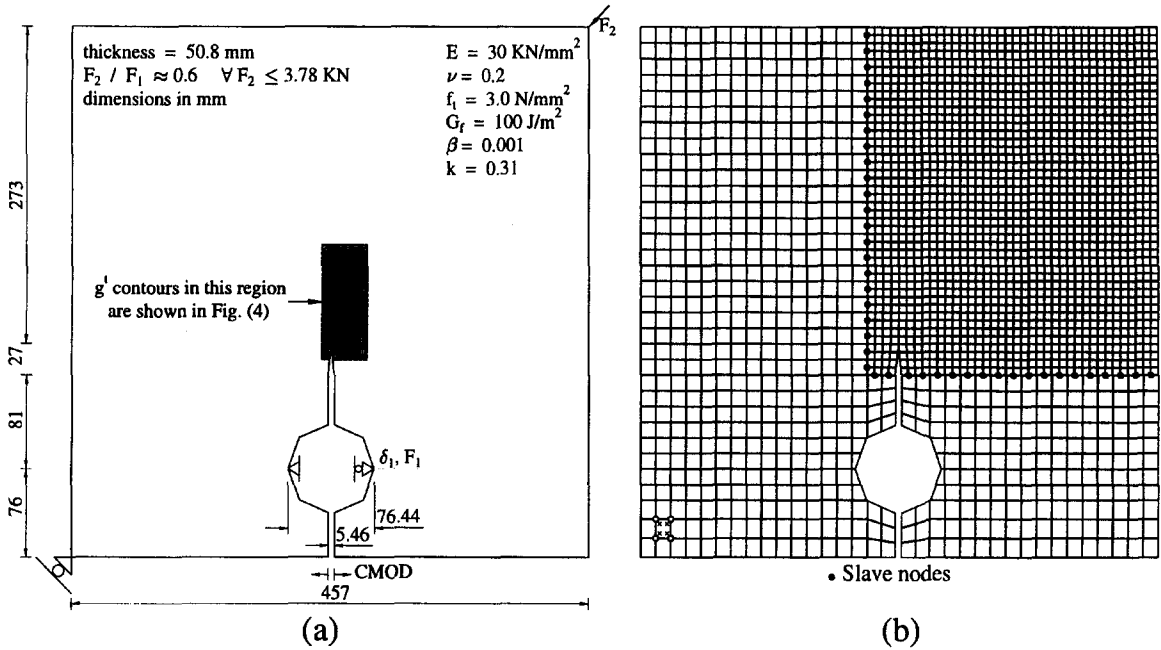
Fig. 2 Crack-line-wedge-loaded double-cantilever-beam (CLWL-DCB) specimen: (a) dimensions, boundary conditions and material properties; (b) finite element mesh.

(a)   (b)
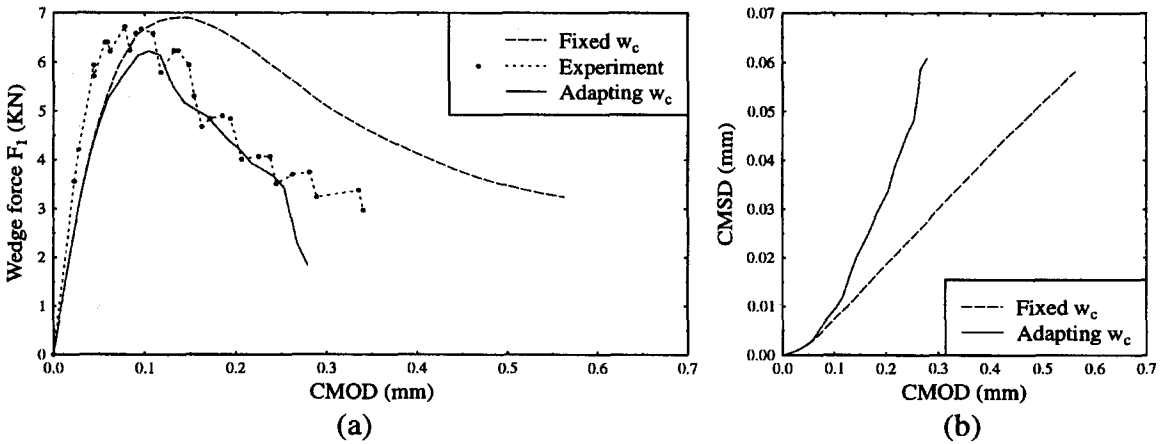
Fig. 3 CLWL-DCB results: (a) wedge force versus CMOD; (b) CMSD versus CMOD.

A solution to this problem consists of freezing the value of w_c. This technique is currently under investigation. The corresponding results for the crack mouth sliding displacement (CMSD) versus the CMOD are illustrated in Fig. 3(b), which clearly shows the difference of the curve considering the adapted w_c from that with constant w_c.
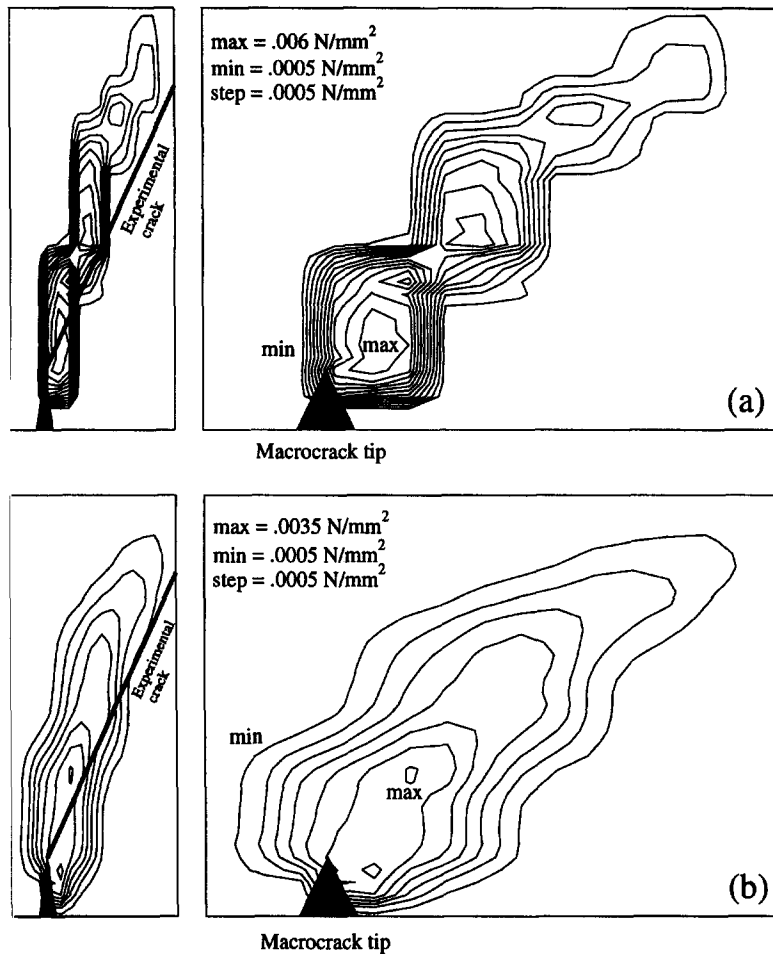
Fig. 4 CLWL-DCB results: (a) contour plot for $\hat{g}^t$; (b) contour plot for $\bar{g}^t$.

Fig. 4 shows contour plots for the apparent fracture energy density before (Fig. 4(a)) and after (Fig. 4(b)) smoothing. The region considered for these plots is the shaded area in Fig. 2(a). It should be noted that these plots are shown in a distorted scale for clarity of the distributions. The non-smoothed contour (Fig. 4(a)) tends to follow the mesh pattern. This reflects one of the main deficiencies of smeared cracking models, which cannot properly capture mixed mode cracking when the fracture zig-zags through the mesh. In this case there is a tendency for the cracks to propagate parallel to the element boundaries (mesh bias). This problem is circumvented by the smooth contour plot of Fig. 4(b).

7. Concluding remarks

The smeared cracking formulation with softening involves the introduction of the *crack band width*. Traditionally, this characteristic length has been determined using ad hoc rules. A systematic

procedure to determine the evolution of this parameter during the nonlinear numerical analysis has been presented here. It is based on the incremental finite element solution and the idea of nonlocal continuum. The required nonlocal forms for the apparent fracture energy density and the crack strains are obtained by means of the superconvergent patch recovery procedure, which makes the computations efficient for practical applications. Thus, the present methodology is potentially advantageous for three dimensional computations. The results obtained indicate the superiority of the present formulation over the standard smeared cracking, and show that the new technique is promising for solving challenging problems of localized fracture such as those involving mixed mode cracking.

Acknowledgements

References

[1] J.G. Rots, Computational modeling of concrete fracture, PhD dissertation, Delft Univ. of Techn., 1988.
[2] Z.P. Bažant, Crack band model for fracture of geomaterials, in: Z. Eisenstein (ed.) Proc. 4th Int. Conf. on Numer. Methods in Geomechanics, Edmonton, Alberta, Canada, 1982.
[3] J. Oliver, A Consistent characteristic length for smeared cracking models, Int. J. Numer. Methods Eng. 28 (1989) 461–474.
[4] D.R.J. Owen, D. Perić, E.A. de Souza Neto, J. Yu, M. Dutko, Advanced computational strategies for 3-D large scale metal forming simulations, in: S.-F. Shen, P.R. Dawson (Eds.) Proc. 5th Int. Conf. on Numer. Methods in Industrial Forming Processes – NUMIFORM'95, Ithaca, NY, 18–21 June, pp. 7–22, 1995.
[5] Y.R. Rashid, Analysis of prestressed concrete pressure vessels, Nucl. Eng. Des. 29(4) (1968) 334–344.
[6] A.H. Nilson et al. (Eds.). State-of-the-art report-finite element analysis of reinforced concrete, ASCE, New York, 1982.
[7] A. Hillerborg, M. Modéer, P.E. Petersson, Analysis of crack formation and crack growth in concrete by means of fracture mechanics and finite elements, Cement Concr. Res. 6(6) (1976) 773–782.
[8] Z.P. Bažant, B.H. Oh, "Crack band theory for fracture of concrete, Materials and Structures, RILEM 16(93) (1983) 155–177.
[9] H.W. Reinhardt, Fracture mechanics of an elastic softening material like concrete, Heron, 29(2) (1984).
[10] Z.P. Bažant and F. Lin, Nonlocal smeared cracking model for concrete fracture, J. Struct. Eng. ASCE 114(11) (1988) 2493–2510.
[11] O.C. Zienkiewicz, J.Z. Zhu, The superconvergent patch recovery and a posteriori error estimates. Part 1: the recovery technique, Int. J. Numer. Methods Eng. 33 (1992) 1331–1364.
[12] A.S. Kobayashi, M.N. Hawkins, D.B. Barker, B.M. Liaw, Fracture process zone of concrete, in: S.P. Shah(Ed.) Application of Fracture Mechanics to Cementitious Composites, Martinus Nijhoff Publ., Dordrecht, pp. 25–50, 1985.